Molecular Vision 2015; 21:749-766 <http://www.molvis.org/molvis/v21/749>
Received 28 January 2015 | Accepted 12 July 2015 | Published 14 July 2015

Astrocytes in the optic nerve head express putative mechanosensitive channels

Hee Joo Choi, Daniel Sun, Tatjana C. Jakobs

Department of Ophthalmology, Harvard Medical School, Massachusetts Eye and Ear Infirmary, Boston, MA

Purpose: To establish whether optic nerve head astrocytes express candidate molecules to sense tissue stretch.
Methods: We used conventional PCR, quantitative PCR, and single-cell reverse transcription PCR (RT–PCR) to assess the expression of various members of the transient receptor potential (TRP) channel family and of the recently characterized mechanosensitive channels Piezo1 and 2 in optic nerve head tissue and in single, isolated astrocytes.
Results: Most TRP subfamilies (TRPC, TRPM, TRPV, TRPA, and TRPP) and Piezo1 and 2 were expressed in the optic nerve head of the mouse. Quantitative real-time PCR analysis showed that TRPC1, TRPM7, TRPV2, TRPP2, and Piezo1 are the dominant isoforms in each subfamily. Single-cell RT–PCR revealed that many TRP isoforms, TRPC1–2, TRPC6, TRPV2, TRPV4, TRPM2, TRPM4, TRPM6–7, TRPP1–2, and Piezo1–2, are expressed in astrocytes of the optic nerve head, and that most astrocytes express TRPC1 and TRPP1–2. Comparisons of the TRPP and Piezo expression levels between different tissue regions showed that Piezo2 expression was higher in the optic nerve head and the optic nerve proper than in the brain and the corpus callosum. TRPP2 also showed higher expression in the optic nerve head.
Conclusions: Astrocytes in the optic nerve head express multiple putative mechanosensitive channels, in particular the recently identified channels Piezo1 and 2. The expression of putative mechanosensitive channels in these cells may contribute to their responsiveness to traumatic or glaucomatous injury.

In glaucoma, retinal ganglion cells degenerate and die, leading to visual impairment or blindness [1]. A leading hypothesis for the pathogenesis of glaucoma implicates the optic nerve head (ONH), and in particular the region of the lamina cribrosa. The rigid lamina cribrosa is an anatomic bottleneck, and in this region, blockage of axonal transport as a result of increased intraocular pressure (IOP) has been demonstrated in various species [2-4]. However, a collagenous lamina cribrosa is not necessary for the development of glaucoma. Mice do not contain any collagen other than collagen IV associated with blood vessels in their ONH, yet they can develop the disease [5-7]. In rodents, as in primates, blockage of axonal transport has been demonstrated in the ONH region [8,9]. In mice, as in primates, the unmyelinated axons in the ONH are directly surrounded by a meshwork of glial fibrillary acidic protein (GFAP)-positive astrocytes. These astrocytes form glial tubes around the axons and organize them into bundles [7]. In a cross section, the astrocytes form a honeycomb structure with pores through which the axons thread. This structure has been called the “glial lamina” [10]. The individual astrocytes that make up the glial lamina are a unique type that is morphologically different from other white matter astrocytes. These astrocytes are large, often spanning the whole diameter of the nerve, and combine their processes to form the glial pores that separate axon bundles [7,11]. As a response to injury, be it traumatic from optic nerve crush or glaucomatous, the astrocytes in the ONH become reactive. This is characterized by profound changes in morphology and gene expression [11-18]. However, what causes astrocytes to become reactive in glaucoma? A possible mechanism would be that if ganglion cells are injured, e.g., by high IOP, they release a distress signal that is picked up by astrocytes and causes them to assume a reactive phenotype. An alternative possibility is that astrocytes directly sense elevated IOP and become reactive in response to the pressure. We have recently demonstrated that a relatively mild, reversible increase of IOP to 30 mmHg for 1 h led to morphological signs of astrocyte reactivity 3 days later. These morphological changes eventually fully resolved by 6 weeks after the pressure spike [19]. At the same time, there was no apparent damage to the ganglion cell axons, which retained a normal structural and ultrastructural appearance and did not show defects in axonal transport [19]. This suggests that astrocytes can become reactive without overt neuronal damage, and the elevation of IOP in itself may be a trigger.

The question of whether the astrocytes of the optic nerve head may be directly sensitive to pressure or stretch has been addressed in cell culture systems. ONH astrocytes in cell culture react to an elevation of orthostatic pressure with changes in gene expression, cell morphology, and cell migration [20-25]. If astrocyte cultures are subjected to

Correspondence to: Tatjana C. Jakobs, Schepens Eye Research Institute, 20 Staniford Street Boston, MA, 02114; Phone: (617) 912-0205; FAX: (617) 912-0116; email: Tatjana_Jakobs@meei.harvard.edu

cyclical stretch, several pathways are induced that are also implicated in astrocyte reactivity, such as the transforming growth factor-β1 (TGF-β1) pathway [26].

Several candidate molecules may confer mechanosensitivity on optic nerve astrocytes. One class of these molecules are the transient receptor potential (TRP) channels. There are 28 *TRP* channel genes in mammals coding for transmembrane proteins of at least six transmembrane domains. Four subunits assemble and form non-selective cation channels, which are Ca^{2+}-permeable [27]. Several members of the TRP channels have been implicated in mechanosensation [28-31]. All TRP channels are apparently expressed in the retina, at least at the transcript level [32]. Though the exact physiologic role for each TRP channel in the retina is not yet known, they obviously play important roles in visual processing, an example being the utilization of TRPM1 in ON bipolar cell signaling [33,34]. Retinal ganglion cells express TRP channels, notably TRPV1 and TRPV2 [35], and TRPV1-mediated Ca^{2+} influx has been shown to contribute to apoptosis in ganglion cells subjected to elevated pressure [36]. However, knockout or inhibition of TRPV1 is not beneficial for retinal ganglion cells since under these conditions, the cells and their axons are more vulnerable to glaucomatous degeneration [37,38]. Another channel through which ganglion cell apoptosis may be mediated is TRPV4 [39]. The glial components of the retina also have been shown to express TRP channels, for example, TRPV1 in microglia [40] and retinal astrocytes, where it mediates cytoskeletal rearrangement and cell migration in response to injury [41]. Taken together, TRP channels may be involved in several aspects of glaucoma, such as the direct response of ganglion cells to increased IOP, astrocyte activation, and the production of cytokines by microglia [28,29,42-45].

Another class of mechanically activated cation channels are the proteins Piezo1 and Piezo2 (also known as Fam38A and Fam38B, respectively). Expression of Piezo1 was discovered in the bladder, colon, kidney, lung, and skin, whereas Piezo2 seems to mediate mechanically activated currents in dorsal root ganglion and trigeminal ganglion cells [46,47], in epidermal Merkel cell complexes [48-52], and in zebrafish light touch receptors [53]. Both Piezos are pore-forming transmembrane proteins, which are non-selective cation channels as well [54,55]. They can apparently function independently of accessory molecules [54]; however, in coimmunoprecipitation experiments Piezo1 has been shown to interact with TRPP2, which inhibits its activity [56]. Both Piezos can also associate with stomatin-like protein 3, increasing their sensitivity to mechanical stimuli [57]. Piezo channels also profoundly influence cell morphology and migration [58-61]. This is of interest in our context, because Piezo channels may be involved in linking increased IOP to the morphological changes that are observed in optic nerve astrocytes [19].

Here we determined the mRNA expression of TRP and Piezo channels in the ONH of C57BL/6 mice. Astrocyte-specific enrichment of the genes was evaluated using single-cell RT–PCR. After that, the expression levels of the mechanosensitive channel candidates that are expressed in many ONH astrocytes were compared in different mouse strains (C57BL/6, the glaucoma-prone DBA/2J strain, and DBA/2J Gpnmb+ as a non-glaucomatous control of the same genetic background as DBA/2J). Expression changes were also examined after transient elevation of the IOP, optic nerve crush, and in glaucomatous DBA/2J mice. We found that several subtypes of TRP channels are expressed in ONH astrocytes, in addition to Piezo1 and 2.

METHODS

Animals: All animals were handled in accordance with the ARVO Statement for the Use of Animals in Ophthalmic and Vision Research, and the procedures were approved by the Institutional Animal Care and Use Committee at Massachusetts Eye and Ear Infirmary. Male and female C57BL/6 mice were purchased from Charles River Laboratories (Wilmington, MA) and used at 6–8 weeks of age. Transgenic mice (hGFAPpr-tomato) in which optic nerve and brain astrocytes express red fluorescent protein were generated by crossing B6;129S6-Gt(ROSA)26Sor$^{tm9(CAG\text{-}tdTomato)Hze}$/J mice (Jackson Laboratories, Bar Harbor, ME) with a mouse line expressing Cre recombinase under the control of the human GFAP promoter. DBA/2J mice were obtained from Jackson Laboratories. We used young (preglaucomatous) DBA/2J mice to assess the expression of the channel genes under normal conditions. These mice were 2–3 months old. We also aged DBA/2J mice to 10 months in our facility. DBA/2J mice develop glaucoma with age, and at 10 months, about a third of the animals show moderate glaucoma, and another third have severe disease [62]. The DBA/2J Gpnmb+ mice (aged 2–4 months) were used as a genetically matched control for DBA/2J in the experiment to examine strain-specific differences in gene expression levels. All strains used were housed on a 12 h: 12 h light-dark cycle and given free access to water and food.

Transient and moderate elevation of IOP: C57BL/6 mice were anesthetized with an intraperitoneal injection of 100 mg/kg ketamine and 20 mg/kg xylazine. The anterior chamber of one eye was cannulated, and the IOP was raised to 30 mmHg as described previously [19]. This level did not cause retinal ischemia and overt damage to the optic nerve axons [19].

The contralateral eye remained untreated and was used as a control.

Optic nerve crush: Unilateral optic nerve crush was performed on the C57BL/6 mice. The conjunctiva at the superior pole of the globe was incised, and the retrobulbar optic nerve was visualized with blunt dissection between the external eye muscles with forceps. The optic nerve was clamped approximately 500 µm behind the globe for 10 s with self-closing jeweler's forceps [11,16]. The optic nerve of the contralateral eye served as a control.

Tissue preparation: Mice were sacrificed by CO_2 asphyxiation followed by decapitation. The skull was opened, and the brain was cut away, leaving the optic nerves in place. Some whole brains of the C57BL/6 mice were sectioned into smaller pieces and stored in RNAlater (Ambion, Carlsbad, CA). If needed, the corpus callosum (CC) was further microdissected from the coronal brain sections. Eyes with optic nerves attached were dissected from the surrounding tissue. The ONHs including the glial lamina were identified under the dissection microscope by the transparency of their unmyelinated axons [7]. The ONHs were separated from the myelinated portion of the optic nerve at the myelination transition zone (approximately 120–170 µm behind the sclera), and all visible remnants of the sclera and the pigmented epithelium were removed under microscopic control. The ONHs and the optic nerve proper (ONP, referring to the myelinated region of the optic nerve) were cut out and stored in RNAlater separately. For the glaucomatous DBA/2J eyes, the retinas were whole-mounted ganglion cell side up on type AA nitrocellulose filters (MF-Millipore; Millipore, Billerica, MA) and fixed in place with 4% paraformaldehyde in PBS (1X; 8.06 mM Na_2HPO_4, 1.94 mM KH_2PO_4, 2.7 mM KCl, 137 mM NaCl, pH 7.4) for 1 h. The retina, kidney, and dorsal root ganglia were used as positive controls for mRNA expression for several of the tested genes. Dorsal root ganglia were harvested according to published procedures and stored in RNAlater [63].

Grading of glaucomatous degeneration in DBA/2J mice: Whole mounts of DBA/2J retinas were used in immunohistochemistry with an antibody against neurofilaments (SMI32, Covance, Dedham, MA). Staining with this monoclonal antibody is a sensitive marker of axon loss and can be used to grade the severity of the ganglion cell loss in the retina [13,64]. The fixed retinas as described above were blocked in 4% normal donkey serum and 0.1% Triton X-100 in PBS at 4 °C overnight and incubated with mouse anti-SMI32 (1:100) at 4 °C for 3 days and then visualized with a secondary antibody conjugated to tetramethyl rhodamine (1:200; Jackson Immunoresearch Laboratories, West Grove, PA). Images of each retina were taken on a BX51 microscope equipped with epifluorescence (Olympus, Center Valley, PA). Retinas were graded as showing no or early glaucoma (NOE), moderate disease (<50% axon loss), and severe disease (≥50% axon loss).

RNA preparation and cDNA synthesis: Tissues from the brain, CC, retina, ONP, kidney, and dorsal root ganglia were removed from the RNAlater solution and immediately placed in the lysis buffer. Due to the small amount of tissue from the ONHs, three ONHs were pooled together to extract RNA for one sample. The total RNA of the brain, CC, retina, ONP, kidney, and dorsal root ganglia was extracted using the RNeasy Plus Mini Kit (Qiagen, Valencia, CA), whereas the total RNA of the ONH was extracted using the RNeasy Plus Micro Kit (Qiagen) due to the small tissue volume. The purity and quantity of RNA were assessed using the NanoDrop 2000 (Fisher Scientific, Pittsburgh, PA), and the RNA integrity was determined on the BioAnalyzer (Agilent Technologies, Santa Clara, CA). Only the RNA samples that had a 260/280 ratio >1.8 and an RNA integrity number (RIN) higher than 5 (mean RIN of 8.16±0.27) were used for cDNA synthesis. Ten nanograms of RNA from the ONHs was reverse-transcribed using the Ovation qPCR System (NuGen, San Carlos, CA), whereas 25 ng of RNA samples from the brain, CC, retina, ONP, kidney, dorsal root ganglia, and some ONH were reverse-transcribed using the SuperScript First-Strand Synthesis System (Invitrogen, Carlsbad, CA) according to the manufacturer's instructions.

Conventional and quantitative PCR: Primers were designed for *TRPC1–7*, *TRPM1–8*, *TRPV1–6*, *TRPP1–3*, *TRPA1*, *Piezo1–2*, and *glyceraldehyde 3-phosphate dehydrogenase (Gapdh)* to span at least one intron/exon boundary using NCBI's Primer-BLAST. Primer sequences for some TRP channels were taken from a published study [65]. Primer sequences are given in Appendix 1. To determine the presence of putative mechanosensitive channels, conventional PCR was performed with AmpliTaq Polymerase in the GeneAmp PCR System 9700 (Applied Biosystems, Carlsbad, CA). Three microliters of undiluted cDNA was used to amplify the TRP and Piezo sequences in a 20 µl reaction volume. *Gapdh* was used as a positive control. The thermocycling conditions were as follows: 9 min at 94 °C, followed by 40 cycles of 30 s at 94 °C, 30 s at 56 °C, and 2 min at 68 °C. The final elongation step was 7 min at 68 °C. After conventional PCR, the amplicons were resolved on 1.5% agarose gels. Bands were excised from the gels and purified using a QIAquick gel extraction kit (Qiagen). The purified DNA was sequenced in the Sequencing Core Facility of the Massachusetts Eye and Ear Infirmary. For the TRP channel genes that had detectable

expression in the ONH, quantitative PCR primers were designed as described above. Information about some primer sequences was obtained from PrimerBank [66] (Appendix 2). The primer and probe sets of TaqMan assays were purchased from Applied Biosystems for the Piezo channels and reference genes (Appendix 3). The cDNA samples that were synthesized using the Ovation qPCR System (NuGen, San Carlos, CA) were diluted at 1:50 and used for quantitative PCR on a StepOnePlus qPCR thermocycler (Applied Biosystems). For the cDNA samples that were synthesized using the SuperScript First-Strand Synthesis System (Invitrogen), 1:2 and 1:10 DNA dilutions were prepared to detect the genes for Piezo and TRPP, respectively. Each reaction for the SYBR Green-based assay contained 2 µl DNA, 1 µl of a mixture of forward and reverse primers, 5 µl of SYBR Green PCR Master Mix (Applied Biosystems), and 1 µl of distilled deionized (dd) water. For TaqMan assays, 4 µl of cDNA was added to 16 µl of the Master Mix containing 1 µl of a predesigned primer/probe set, 10 µl of TaqMan Gene Expression Master Mix (Applied Biosystems), and 5 µl of dd water. The quantitative PCR conditions were as follows: 10 min at 95 °C, followed by 40 cycles of 15 s at 95 °C and 1 min at 60 °C. Melting curve analysis following SYBR Green-based detection confirmed the specificity of the amplification and the absence of nonspecific amplification and primer dimers. Genomic DNA was removed during RNA extraction using a gDNA Eliminator spin column in the RNeasy Plus Micro and Mini Kits, and the primers that cross intron/exon boundaries were used to avoid amplifying genomic DNA. Some samples omitting the reverse transcription step (NRT controls) were run to confirm that no genomic DNA contamination was detected. *Gapdh* was used as a reference gene in most quantitative PCR experiments since the expression level in the ONH is stable after an increase in IOP or optic nerve crush [15,16]. For a comparison of the TRPP and Piezo expression levels between different tissues, however, *peptidylprolyl isomerase A (Ppia)* was used as a reference gene instead of *Gapdh* because previous in situ hybridization studies showed that *Gapdh* mRNA level in neurons is much higher than that in glial cells in the brain [67,68]. The expression stability of three reference genes, *Gapdh*, *Ppia*, and β-actin *(Actb)*, between four tissues (ONH, brain, CC, and ONP) was analyzed with Normfinder [69] and BestKeeper [70]. Both software identified *Ppia* as the best reference gene for the experiment. At least three biologic replicates (mostly five to six samples) were used for each condition, and all samples were run in triplicate with non-template control.

Isolation of single astrocytes and single-cell RT–PCR: Collection of individual astrocytes and single-cell RT–PCR were performed according to a protocol first established to isolate retinal neurons [71-73]. Two ONHs of the C57BL/6 mice were incubated for 25 min in Hank's balanced salt solution (HBSS) containing 21 U/ml papain (Worthington, Lakewood, NJ) and L-cysteine (10 mg/ml), and then washed with HBSS containing 10% horse serum and 60 U/ml DNase. The tissue was triturated with a series of heat-polished Pasteur pipettes to dissociate it into single astrocytes. Under a Zeiss Axiovert 200 (Carl Zeiss Microscopy, Peabody, MA) microscope, single astrocytes were visualized and aspirated with a silanized glass micropipette and then expelled into sterile PBS with 2% bovine serum albumin (BSA) for washing. Then the cell was transferred with a new glass micropipette into a thin-wall reaction tube containing reaction buffer and all the outer primers. A sample of washing buffer (2% BSA in PBS) was also taken as a negative control. The reverse transcription and the first-round PCR were done in the same tube using AMV Reverse Transcriptase and Tfl polymerase (Access RT–PCR System, Promega, Madison, WI). A second round of PCR was run with nested primers for each gene. The TRP channel genes and Piezo1 and 2 that had been examined in the conventional PCR experiments were tested again. In addition, we tested each isolated cell for the expression of GFAP to verify that the cell was an astrocyte, and for the expression of myelin basic protein (MBP) and CD45, as negative controls, to ensure that the cell was not contaminated with other components of the ONH such as oligodendrocytes or microglia. One-sixtieth of the first-round reaction product was used as a template, and the target sequence was amplified using AmpliTaq Polymerase. Primer sequences and amplicon sizes are given in Appendix 1.

Data analysis: The $2^{-\Delta\Delta CT}$ method was used to analyze quantitative PCR data. Statistical comparisons of the expression levels of the TRP and Piezo genes were performed with the ΔCt values that were averages of three technical replicates. Statistical significance between the control and experimental groups was determined using a two-tailed Student *t* test whereas one-way ANOVA was used for comparisons between multiple groups, followed by a Tukey post-hoc test. For the data analysis of gene expression in various mouse strains (C57BL/6, DBA/2J, DBA/2J Gpnmb+), Kruskal-Wallis ANOVA and the Mann-Whitney test were used as the nonparametric alternative due to the small sample size of DBA/2J Gpnmb+ mice (n=3). Similarly, the Wilcoxon signed-rank test and the Mann-Whitney test were used to analyze results in different models of optic nerve damage (n=3 for each condition). All statistical analyses were performed using OriginPro (OriginLab, Northampton, MA) and MATLAB (MathWorks, Natick, MA). $p<0.05$ was considered statistically significant. To present relative gene expression in a graph, each ΔCt

value was transformed by the $2^{-\Delta\Delta CT}$ calculation. All data are expressed as the mean ± standard error of the mean (SEM).

RESULTS

Putative mechanosensitive channels are expressed in the ONH: To examine whether astrocytes in the ONH can directly sense an increase in IOP, we first determined the presence of putative mechanosensitive channels in the ONH using conventional PCR. The TRP and Piezo channels were chosen as the candidate genes because they have been implicated in mechanosensation in other tissues [30,31,46,74]. The mammalian TRP family is subdivided into six subfamilies. Five (TRPC, TRPM, TRPV, TRPA, and TRPP) of the six TRP subfamilies and two Piezo channels were examined in the ONH of the C57BL/6 mice. TRPML was not examined in this study because the TRP subfamily functions as an intracellular channel in endosomes and lysosomes [74]. Figure 1 and Table 1 show that most TRPC and TRPM channels (except TRPC7, TRPM5, and TRPM8), two TRPV channels (TRPV2 and 4), TRPA1, TRPP1–3, and both Piezo channels are expressed in the ONH. TRPP1 and TRPP2 as used here are polycystic kidney disease 1 (PKD1), a TRP-associated protein interacting with TRPP2, and PKD2, respectively. Although three TRPP channels (TRPP2, TRPP3, and TRPP5) are reported in mammals [27], TRPP5 (PKD2L2) was not examined because its expression is mainly restricted to the testes [75] whereas TRPP3 (PKD2L1) is widely expressed [76-78].

Given the role that TRPV1 plays in retinal ganglion cells and astrocytes, we were surprised that no TRPV1 transcripts were detectable in the optic nerve head. However, in several preparations of cDNA from the ONH, TRPV1 was undetectable, whereas in cDNA from the brain and the whole retina assayed under the same conditions a clear signal was detected (Appendix 4). RNA transcripts for TRPC7, TRPV5, TRPV6, TRPM5, and TRPM8 were also detected in positive control tissues such as the brain, retina, kidney, and dorsal root ganglia (Appendix 4). We then sought to determine which channels are highly expressed on the mRNA level in the ONH of C57BL/6 mice. Therefore, quantitative real-time PCR was performed to determine the relative significance of each mechanosensitive channel that was detected in conventional PCR (Table 1). The expression levels of the TRPA1 and TRPP3 channels were extremely low in our preliminary study; thus, both genes were not further examined. In each biologic replicate, the mRNA levels of each TRP and Piezo gene were normalized to one gene in the same subfamily that showed a moderate expression level, and then the values of the normalized expression level were averaged to obtain the mean and the SEM.

As shown in Figure 2A, TRPC1 is the most abundant isoform in the TRPC subfamily. The relative mRNA level was 227.70±84.82 (n=6) compared to TRPC2 expression, and the gene expression was significantly higher than that of all other TRPC channels ($p<0.001$). The expression levels of TRPC3 and TRPC6 were about 20% of the level of TRPC2. The mean of the TRPC4 mRNA level was similar to TRPC2, but there was high variation among the biologic replicates. One-way ANOVA showed there was no significant difference among the TRPC2, TRPC3, TRPC4, TRPC5, and TRPC6 isoforms except between TRPC2 and TRPC5. TRPC5 showed the lowest expression, and the mRNA level was significantly lower than TRPC2 expression ($p<0.01$).

Despite the high variation among the biologic replicates, TRPM7 is obviously the most abundant isoform in the TRPM subfamily, followed by TRPM3 and TRPM6 (Figure 2B, TRPM7: 38.24±10.67, TRPM3: 6.96±1.98 compared to TRPM6; n=6) although the gene expression levels of TRPM3

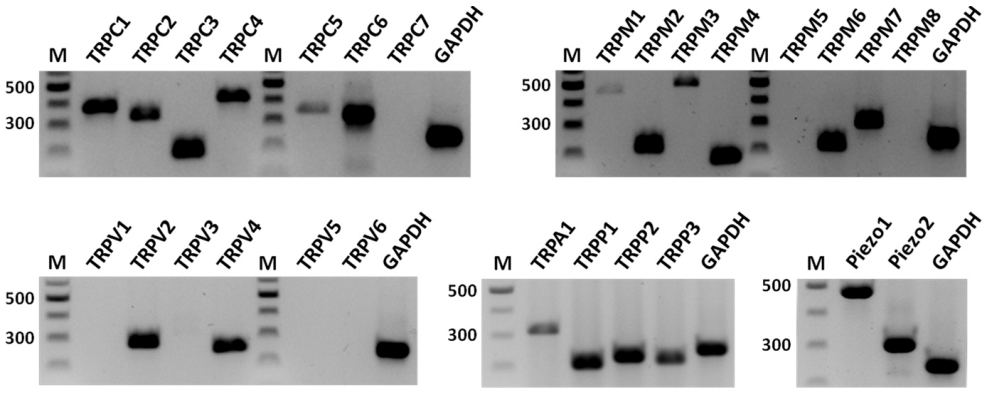

Figure 1. Expression of candidate mechanosensitive genes in the mouse optic nerve head. Twenty-five transient receptor potential (TRP; seven TRPC, eight TRPM, six TRPV, TRPA, three TRPP) and two Piezo channels were examined using conventional PCR. Eighteen TRP (six TRPC, six TRPM, two TRPV, TRPA, three TRPP) and both Piezo channels were detected. *Gapdh* was used as a control. M, DNA length marker (100 bp ladder).

and TRPM6 were not significantly different. The mean of TRPM4 expression was about 9% of TRPC6, and TRPM1 and TRPM2 showed low expression. The mRNA levels of TRPM2 and TRPM4 were significantly lower than those of TRPM3, TRPM6, and TRPM7 ($p<0.001$), but there was no significant difference between TRPM2 and TRPM4. TRPM6 expression was significantly lower than TRPM7 expression ($p<0.01$). The TRPM1 data are not presented in Figure

Table 1. Summary of TRP and Piezo channel mRNA expression.

Gene	Conventional PCR	Single-cell RT–PCR	Quantitative PCR		CC	Brain
	ONH	ONH astrocyte	ONH	ONP		
TRPC channels						
TRPC1	+	+	+	nt	nt	nt
TRPC2	+	+	+	nt	nt	nt
TRPC3	+	-	+	nt	nt	nt
TRPC4	+	-	+	nt	nt	nt
TRPC5	+	-	+	nt	nt	nt
TRPC6	+	+	+	nt	nt	nt
TRPC7	-	-	nt	nt	nt	nt
TRPV channels						
TRPV1	-	-	nt	nt	nt	nt
TRPV2	+	+	+	nt	nt	nt
TRPV3	-	-	nt	nt	nt	nt
TRPV4	+	+	+	nt	nt	nt
TRPV5	-	-	nt	nt	nt	nt
TRPV6	-	-	nt	nt	nt	nt
TRPM channels						
TRPM1	+	-	+	nt	nt	nt
TRPM2	+	+	+	nt	nt	nt
TRPM3	+	-	+	nt	nt	nt
TRPM4	+	+	+	nt	nt	nt
TRPM5	-	-	nt	nt	nt	nt
TRPM6	+	+	+	nt	nt	nt
TRPM7	+	+	+	nt	nt	nt
TRPM8	-	-	nt	nt	nt	nt
TRPA channel						
TRPA1	+	-	nt	nt	nt	nt
TRPP channels						
TRPP1 (PKD1)	+	+	+	+	+	+
TRPP2 (PKD2)	+	+	+	+	+	+
TRPP3 (PKD2L1)	+	-	nt	nt	nt	nt
Piezo channels						
Piezo1 (Fam38a)	+	+	+	+	+	+
Piezo2 (Fam38b)	+	+	+	+	+	+

All results were obtained from C57BL/6 mice or, in the case of the single cell RT–PCRs, from a transgenic, red fluorescent protein-expressing strain that is on the C57BL/6 genetic background. +, signal detectable; -, signal not detectable; nt, not tested; ONH, optic nerve head; ONP, optic nerve proper; CC, corpus callosum.

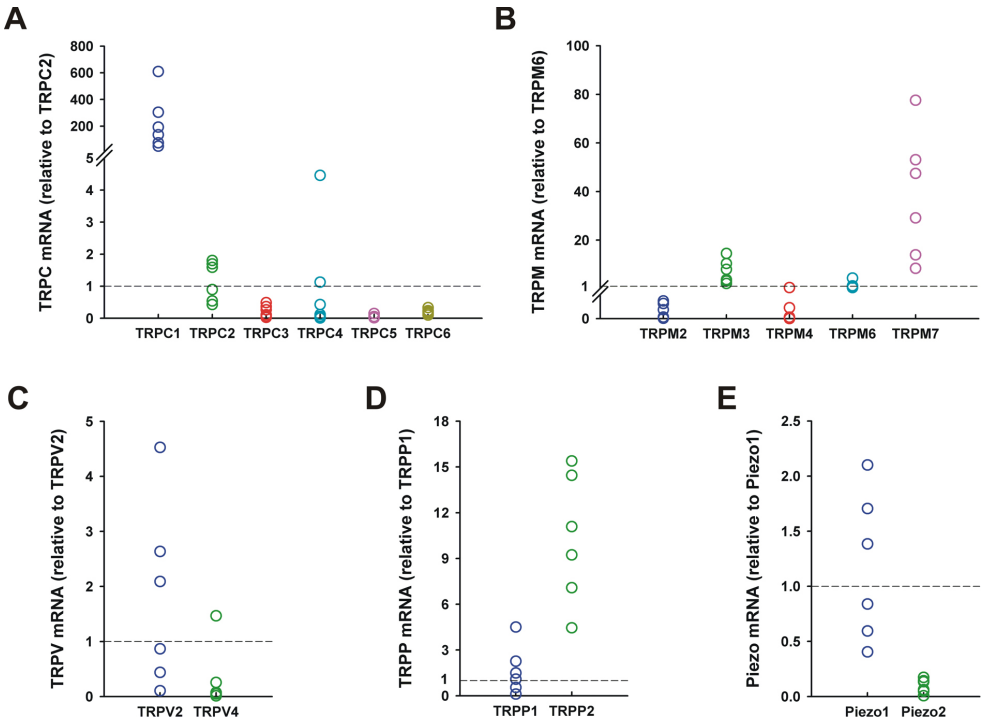

Figure 2. Relative mRNA levels of TRP and Piezo channels in the optic nerve head of C57BL/6 mice (n=6). Expression of 15 transient receptor potential (TRP; six TRPC, five TRPM, two TRPV, two TRPP) and two Piezo genes were determined with quantitative real-time PCR. Data represent fold differences relative to a control gene in the same subfamily: The control genes are TRPC2 for TRPC (**A**), TRPM6 for TRPM (**B**), TRPV2 for TRPV (**C**), TRPP1 for TRPP (**D**), and Piezo1 for Piezo (**E**). Dashed lines represent the mean expression of the control genes.

2B because only one biologic replicate showed TRPM1 expression.

Our conventional PCR results revealed that only two isoforms of the TRPV subfamily, TRPV2 and TRPV4, are expressed in the ONH (Figure 1). TRPV2 showed higher expression than TRPV4 in each biologic replicate, and the difference in averaged gene expression (n=6) was statistically significant ($p<0.05$). Members of the TRPP subfamily were first found in a study of human polycystic kidney disease. TRPP1 is thought of as a mechanical sensor, and this protein interacts with the Ca^{2+}-permeable cation channel TRPP2. In the ONH, the expression level of TRPP2 was significantly higher than TRPP1 (Figure 2D, TRPP2: 10.28±1.73; n=6, $p<0.05$). Piezo channels have been intensively studied in many species and tissues to investigate their functions, but research on the expression and function of Piezos in the retina and the ONH has not been conducted. In the present study, both Piezo channels were expressed in the ONH (Figure 1), and Piezo2 expression was significantly lower than that of Piezo1 in the region (Figure 2E, Piezo2: 0.09±0.03 compared to Piezo1; n=6, $p<0.001$).

Expression of TRP and Piezo channels in ONH astrocytes: Although astrocytes are the major cell type present in the mouse ONH, the ONH contains other components such as retinal ganglion cell axons, microglia, and blood vessels. To examine which subtypes of the mechanosensitive channels that were detected in the whole ONH tissue (Figure 1 and Figure 2) are expressed in astrocytes, we modified our cell dissociation protocol that has been used to isolate subtypes of retinal neurons to perform single-cell RT–PCR on isolated astrocytes. With this protocol, we succeeded in obtaining morphologically intact ONH astrocytes as shown in Figure 3A.

We assayed all five TRP subfamilies and both Piezos in single astrocytes dissociated from the ONH of five wild-type C57BL/6 mice. Only cells that tested positive for the expression of GFAP, but negative for MBP and CD45 were considered for data (n=23, Table 2). TRPC1 (87%), TRPP1 and 2 (78%), and TRPM7 (52%) and Piezo2 (43%) were the most commonly expressed subtypes. RNA transcripts of TRPC2, TRPC6, TRPV2, TRPV4, TRPM2, TRPM4, TRPM6, and Piezo1 were also detected in ONH astrocytes. The astrocyte in Figure 3A showed expression of TRPC1–2, TRPV2, TRPM7, and TRPP1–2, which are highly expressed in the ONH tissue as shown in Figure 2, as well as Piezo2, which is highly expressed in isolated ONH astrocytes as presented in Table 2 (Figure 3B). The results of the single-cell RT–PCR experiments are summarized in Table 2. A previous study implicated TRPC1 as a component of mechanosensitive channels [79], and our present data also showed that TRPC1 is highly expressed in the ONH (Figure 2A) and detected in single astrocytes. However, recent studies have questioned whether TRPC1 is directly gated by pressure

Table 2. Expression of TRP and Piezo channels in single ONH astrocytes (n=23).

Gene	Number of astrocytes (%)	Gene	Number of astrocytes (%)
TRPC1	20 (87%)	TRPP1	18 (78%)
TRPC2	5 (22%)	TRPP2	18 (78%)
TRPC6	3 (13%)	Piezo1	5 (22%)
TRPV2	3 (13%)	Piezo2	10 (43%)
TRPV4	4 (17%)		
TRPM2	1 (4%)		
TRPM4	2 (9%)		
TRPM6	7 (30%)		
TRPM7	12 (52%)		

Single-cell RT–PCR was performed on individual astrocytes dissociated from the ONH of C57BL/6. 33 ONH astrocytes from five C57BL/6 mice were examined and only pure astrocytes (n=23) that were not contaminated with other cell components such as oligodendrocytes were used for gene expression analysis.

or stretch. Smooth muscle cells of TRPC1-deficient mice showed no significant differences in mechanosensation compared to cells from wild-type mice [80]. In addition, co-overexpression of TRPC1 and TRPC6 in African green monkey kidney (COS) or Chinese hamster ovary (CHO) cells failed to confirm the mechanosensitivity of these channels [81]. Though it is possible to identify astrocytes from wild-type mice based on their morphology and the mRNA expression for GFAP, we performed an additional experiment using the ONHs from a transgenic mouse strain that expresses red fluorescent protein in all astrocytes as further proof that the isolated cells are astrocytes. This mouse strain is on the C57BL/6 genetic background (see Materials and Methods). We isolated seven individual astrocytes from three mice of this strain and tested them for the expression of TRPP1–2 and Piezo1–2 and the control genes *(Gfap, Mbp*, and CD45). As expected, the majority expressed TRPP1 and TRPP2 (seven of seven cells), Piezo2 (five of seven cells). Piezo1 was found in two of seven cells.

Expression differences in TRP and Piezo channels between the C57BL/6 and DBA/2J strains: To determine strain-specific differences in TRP and Piezo gene expression, we repeated the quantitative PCR experiments on DBA/2J Gpnmb+ and DBA/2J with no or early glaucoma (NOE). The first and second most highly expressed genes in each TRP subfamily and Piezos that were detected in the ONH astrocytes (Table 2) were examined, and the averaged mRNA levels of each

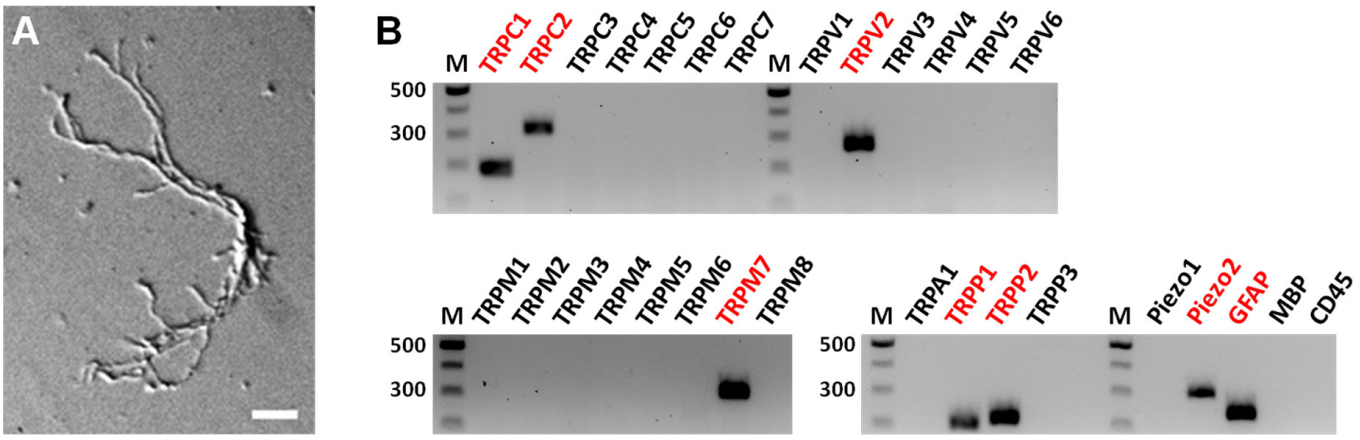

Figure 3. Single-cell RT–PCR analysis of TRP and Piezo channel genes in single optic nerve head astrocytes. **A**: A representative picture of acutely dissociated astrocytes. This cell has the thick, elongated cell body and long primary processes that are the morphology of optic nerve head astrocytes observed in vivo. Scale bar, 20 µm. **B**: 25 transient receptor potential (TRP; seven TRPC, six TRPV, eight TRPM, one TRPA, three TRPP) and two Piezo channel genes were examined. The astrocyte in **A** expresses TRPC1–2, TRPV2, TRPM7, TRPP1–2, and Piezo2 channels. Glial fibrillary acidic protein (GFAP) was used as an astrocyte marker. MBP, an oligodendrocyte marker. CD45, a microglia marker. M, DNA length marker (100 bp ladder).

group were normalized to the same gene of C57BL/6 that is presented in Figure 2. Statistical significance between the three groups was determined using Kruskal–Wallis ANOVA followed by a Mann–Whitney test. The C57BL/6 mice showed higher expression levels of TRPC1, TRPC2, and TRPM7 than the DBA/2J Gpnmb+ and DBA/2J mice (Figure 4A,B). Interestingly, the expression levels of TRPM6 and both Piezos in the DBA/2J mice were higher compared to the C57BL/6 and DBA/2J Gpnmb+ strains (Figure 4B,E). The TRPV and TRPP channels showed similar expression levels in the three mouse strains (Figure 4C,D).

Expression of TRPP and Piezo channels in different tissue regions: We wondered how the expression levels in the ONH compare with those of other central nervous system (CNS) structures, and especially with white matter tracts such as the corpus callosum and the myelinated part in the optic nerve proper (ONP). To address the question, the total RNA was extracted from four tissue regions in the C57BL/6 mice: the ONH, brain, CC, and ONP.

Conventional PCR showed that all the tissues examined expressed TRPP1–2 and Piezo1–2 (Figure 1, Figure 5A, and Table 1). Interestingly, two bands for Piezo2 were detected in the brain, CC, and ONP, suggesting the presence of splice variants in the regions. The weak band appeared at 220–240 bp, shorter than the expected amplicon product (299 bp, upper band). Sequencing confirmed that it was a splice variant of 223 bp. We aligned this sequence with the predicted transcript

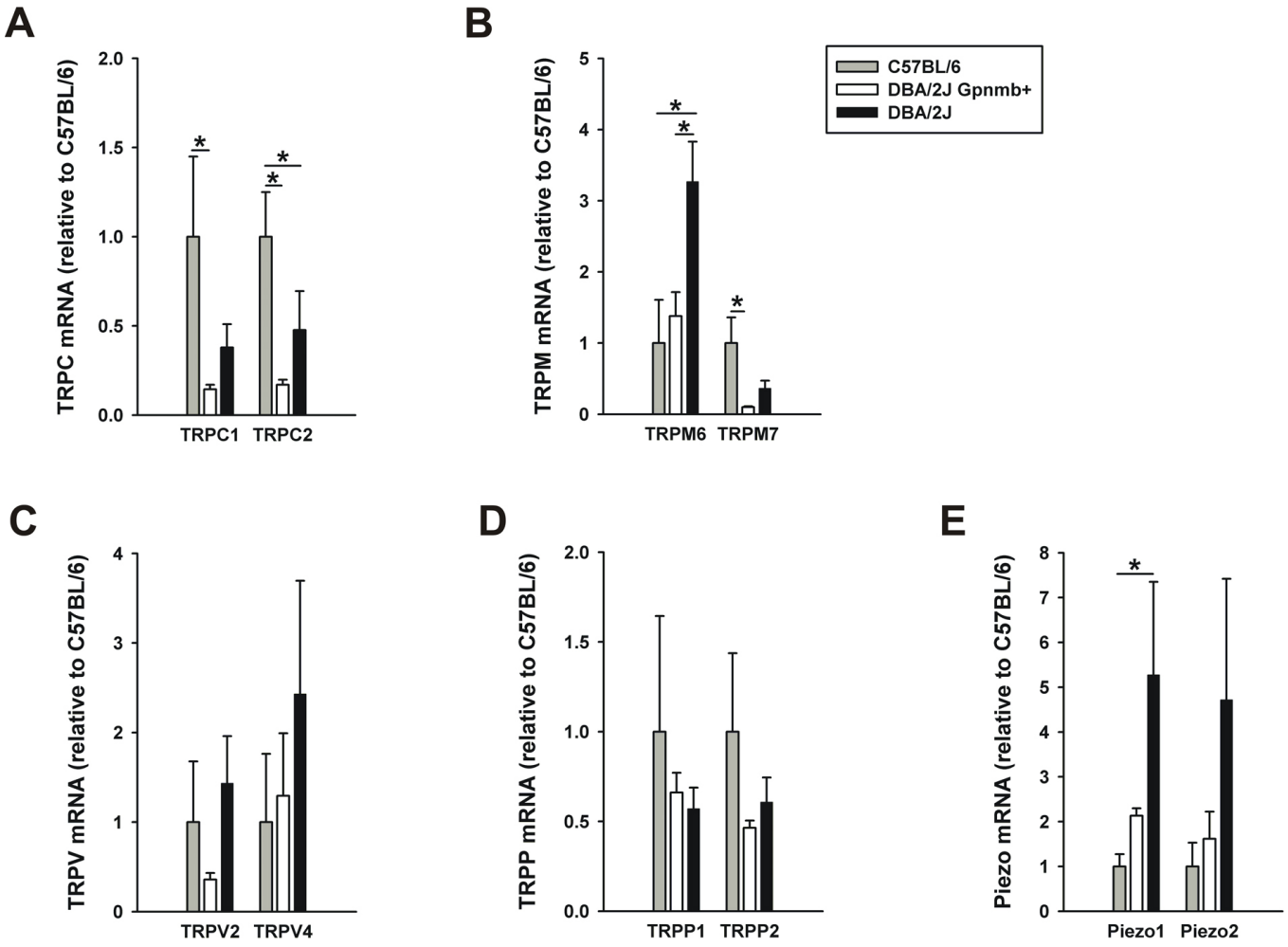

Figure 4. Comparison of TRP and Piezo channel mRNA levels in the optic nerve head between C57BL/6 (n=6, gray bars) and DBA/2J (n=6, black bars) strains. Normal DBA/2J mice with no or early glaucoma were used in this experiment. DBA/2J Gpnmb+ (n=3, white bars) mice were used as another control for DBA/2J. Expression of eight transient receptor potential (TRP) (**A**–**D**) and two Piezo (**E**) genes that were detected in astrocytes dissociated from the optic nerve head were determined with quantitative real-time PCR. Data represent fold differences relative to the same genes of C57BL/6. Significant expression differences for each gene between the three groups were assessed using Kruskal–Wallis ANOVA followed by a Mann–Whitney test. *p<0.05. Error bar, mean ± SEM.

variants of Piezo2 and found it was identical with transcript variant X8 (accession number: XR_386006).

Next, we performed quantitative PCR to compare the expression levels of TRPP and Piezo between the four tissue regions. For this comparison experiment, the total RNA extracted from the ONHs was reverse-transcribed to cDNA using the SuperScript First-Strand Synthesis System that had been used for cDNA synthesis of the brain, CC, and ONP. This ruled out the possibility that using two different reverse-transcription kits could cause different levels of amplification from the same sample. TRPP1 showed a tendency for higher expression levels in the ONH compared to the brain, CC, and ONP (Figure 5B, brain: 0.31±0.11, CC: 0.34±0.07, ONP: 0.39±0.10, n=6 for the ONH and ONP, n=5 for the brain and CC), but only the expression difference between the ONH and the brain was significant. TRPP2 showed a similar expression pattern. The highest expression of TRPP2 was found in the ONH, and the expression levels were significantly lower in the brain, CC, and ONP compared to the ONH (brain: 0.17±0.05, CC: 0.24±0.03, ONP: 0.45±0.05, n=6 for the ONH and ONP, n=5 for the brain and CC). There was also a difference in TRPP2 expression between the brain and the ONP. Taken together, the ONH showed higher expression of TRPP1 and 2 than other gray and white matter regions.

As for Piezo1, there were no expression difference between the four tissue regions except between the brain and the ONP (Figure 5C). The brain showed the lowest level of Piezo2 expression compared to the three other regions. The mRNA level for Piezo2 in the brain was about 15% of the level in the ONH (0.14±0.08, n=5, $p<0.01$). Piezo2 expression was also low in the CC compared to the ONH (0.45±0.07, n=5), but the expression difference between the brain and the ONH was not significant. The ONP showed high expression levels of both Piezos, and there were no significant differences for Piezo1 and Piezo2 between the ONH and the ONP.

Piezo2 is upregulated in optic nerve injury: It was previously reported that the expression of numerous genes changes in the ONH after exposure to elevated IOP in vivo [14,15,17]. If the gene expression of putative mechanosensitive channels in the ONH can also be altered, it could make the region more or less sensitive to IOP. Therefore, we examined whether the expression of TRPP1–2 and Piezo1–2 also changes in three mouse models of optic nerve damage, including glaucoma.

To examine the effect of a mild and transient elevation in IOP on the TRPP and Piezo expression levels, a mouse model of elevated IOP that was demonstrated in our recent work was used [19]. At various time points after an elevation of IOP (1 h, 3 days, 1 week), changes in the TRPP and Piezo mRNA levels were examined. Second, an optic nerve crush injury model was chosen to assess the effect of severe damage to axons and glia on the channel expressions at various time points after injury (1 day, 3 days, 1 week, 3 weeks). Last, glaucomatous DBA/2J mice were used to determine how the expression levels of TRPP and Piezo change in spontaneous glaucoma.

For the TRPP channels, no upregulation was seen in the three mouse models. TRPP1 was downregulated 1 week after short-term elevation in IOP (Figure 6A), and TRPP1 and 2 were downregulated 1 day after the optic nerve crush injury (Figure 6C), but the gene expression changes were not significant. Piezo1 did not show obvious up- or downregulation in any of the three models except 3 days after the crush injury, but Piezo2 showed considerable changes in gene expression. One hour after the elevation of IOP, Piezo2 was downregulated, and the expression level was about 40% of the contralateral control (Figure 6B). In the optic nerve crush model, Piezo2 showed a tendency to be upregulated at most recovery intervals (3 days, 1 week, 3 weeks) although the increases in gene expression were not significant (3 days: 22.43±18.48, 1 week: 7.78±2.35, 3 weeks: 10.39±4.65 compared to the contralateral control; n=3, Figure 6D). The Piezo2 mRNA levels 3 days after the optic nerve crush displayed high variation among the biologic replicates. Piezo2 expression also showed a tendency to be upregulated in moderate and severe glaucoma in the DBA/2J mice, and the relative expression levels were 5.86±3.08 and 7.81±1.92, respectively (n=3). Note that all relative expression levels seen in Figure 6 are presented on a $\log_2$ scale to show up- and downregulation of the genes compared to the control groups.

DISCUSSION

In this study, we addressed the question of whether ONH astrocytes possess the molecular equipment to sense mechanical stress directly. The motivations for this question were twofold. First, in vitro studies of cultured ONH astrocytes demonstrated that they react to an increase in orthostatic pressure or to stretch imparted by growing the cells on deformable membranes and subjecting them to cyclical stretch. It was demonstrated that elevating the orthostatic pressure over a culture of ONH astrocytes induces upregulation of intermediate filament genes such as *Gfap* and *vimentin* [20] and decreases gap junctional coupling by connexin-43 [21]. Rogers and colleagues analyzed the proteome of ONH astrocytes under various conditions of cyclical strain and identified more than 500 differentially expressed proteins, among them several that are associated with astrocyte activation [26,82].

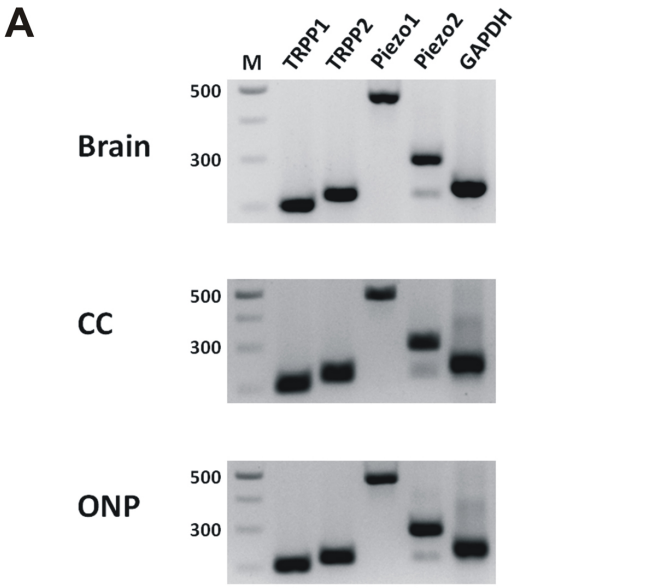

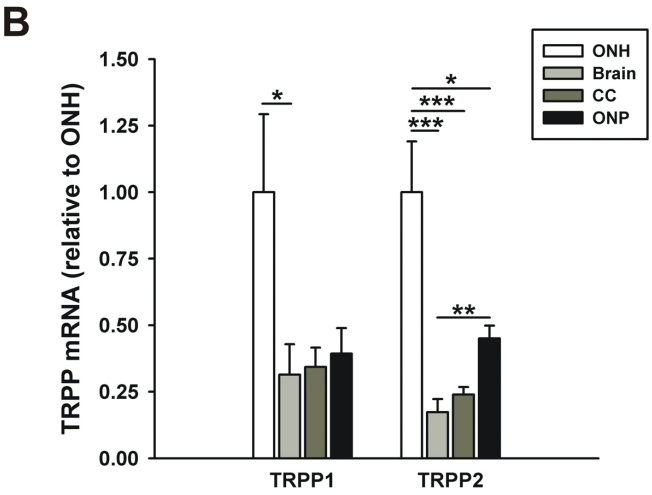

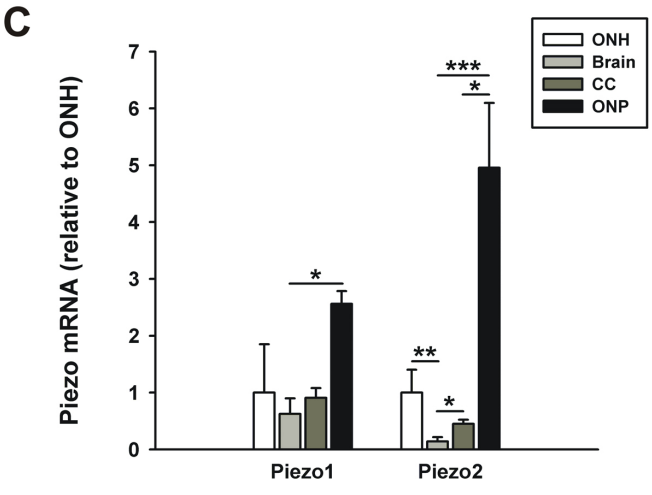

Figure 5. Comparison of TRPP and Piezo channel expression between different tissues. Expression of TRPP1–2 and Piezo1–2 channels in the optic nerve head, brain, corpus callosum, and optic nerve proper of C57BL/6 mice was determined with conventional (**A**) and quantitative real-time PCR (**B** and **C**). **A**: TRPP1–2 and Piezo1–2 were expressed in all the tissues examined. Two splice variants of the *Piezo2* gene were detected. **B** and **C**: TRPP and Piezo mRNA levels in four different tissues are presented as the fold difference relative to the same gene expression in the optic nerve head (n=6 for the ONH and ONP, n=5 for the brain and CC). Significant expression differences for each gene between four tissues were analyzed using ANOVA. *p<0.05, **p<0.01, and ***p<0.001. ONH, optic nerve head; CC, corpus callosum; ONP, optic nerve proper. Error bar, mean ± standard error of the mean (SEM).

Our second motivation for the present study was the recent observation that even a short and relatively mild increase in IOP (30 mmHg for 1 h) leads to morphological signs of astrocyte reactivity in the ONH in the absence of obvious damage to the ganglion cell axons [19]. This suggests that the astrocytes may be reacting to some stimulus that occurs before there is damage to the optic nerve axons, and the pressure itself could be such a stimulus. We hypothesized that astrocytes may directly sense tissue stretch with mechanosensitive channels.

As an effort to understand the mechanisms by which elevated IOP in glaucoma is linked to retinal ganglion cell damage and death, several studies have been conducted to find stretch-activated ion channels, including TRP channels, in the retina and the ONH, which convert membrane strain to biologic signals [32,35-37,39-41,83-88]. For instance, mouse retinal ganglion cells express TRPV4, and sustained activation of this channel using TRPV4 agonists leads to apoptosis of the ganglion cells [39]. Immunohistochemistry performed on vertical retina sections and primary cultures also showed TRPP2 expression in mouse retinal ganglion cells [86]. In particular, TRPV1 mRNA and protein are expressed in several cell types in the retina, such as microglia, photoreceptors, amacrine cells, retinal ganglion cells, and astrocytes, and pressure-induced calcium influx through the TRPV1 channel has been described [36,40,89-92]. Many subfamilies of TRP channels have been implicated in mechanosensation [30,31]. As a step toward seeking putative mechanosensitive channels in ONH astrocytes, we determined the mRNA levels of most TRP subfamilies, and of the directly mechanosensitive Piezo channels. We were particularly interested in the latter because of the involvement of Piezo channels in cell morphology, adhesion, and migration [55]. Astrocytes in the optic nerve react to an increase in IOP with changes in morphology, suggesting that the astrocytes become mobile, or at least rearrange their processes [13,19].

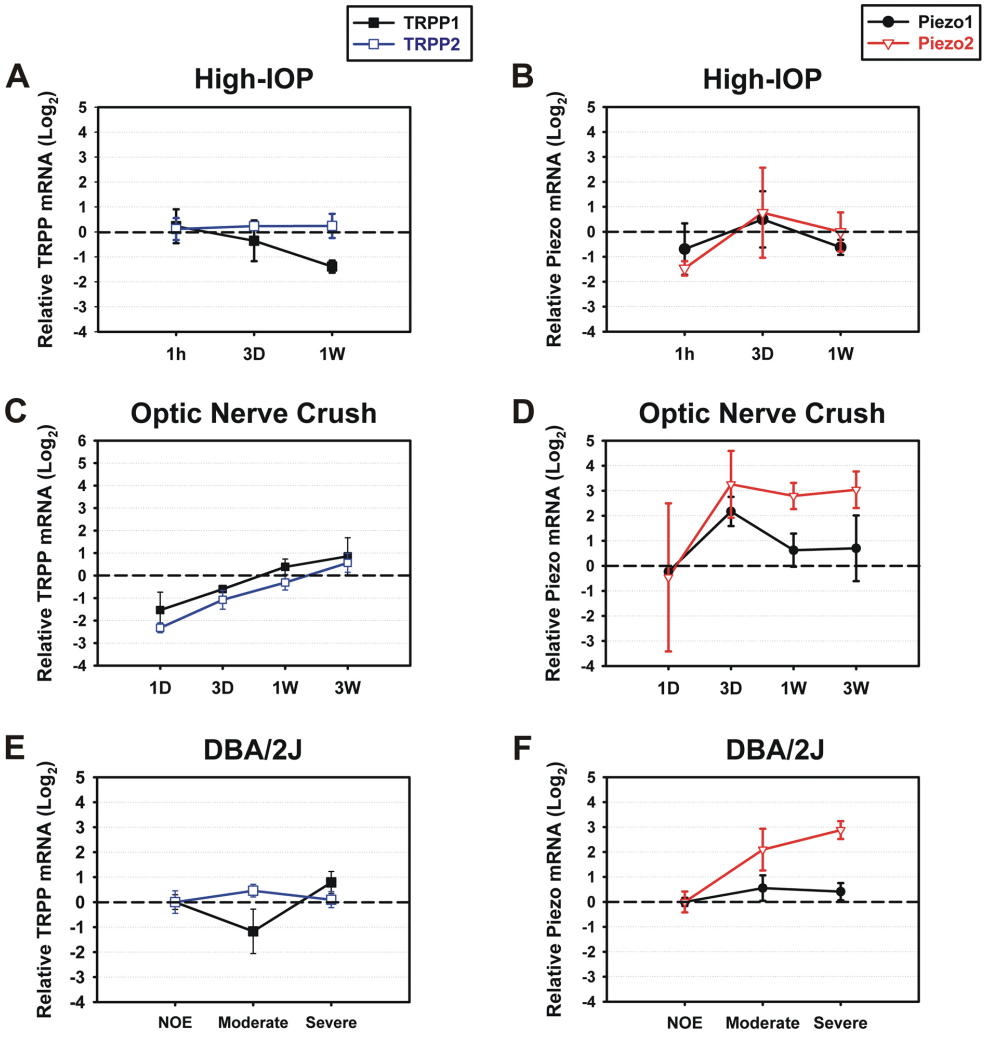

Figure 6. Fold changes in TRPP and Piezo expression levels in three mouse models of optic nerve damage. (**A**–**B**) an elevated intraocular pressure (IOP) model, (**C**–**D**) an optic nerve crush injury model, and (**E**–**F**) glaucomatous DBA/2J mice. Quantitative real-time PCR was performed to assess TRPP and Piezo mRNAs in the optic nerve head prepared from each model (n=3 biologic replicates per time point/severity of glaucoma). The mRNA levels after the elevation in IOP, optic nerve crush, and in glaucomatous degeneration were normalized to the contralateral control eyes (**A**–**D**) and control animals with no or early glaucoma (NOE; **E**–**F**), and then presented on a $\log_2$ scale. Dashed lines represent the mRNA levels of transient receptor potential (TRP) TRPP and Piezo channels in the control groups. Error bar, mean ± SEM.

Our results show that many TRP channels and both Piezos are expressed in the ONH, and single-cell RT–PCR demonstrated the presence of TRPC1–2, TRPC6, TRPV2, TRPV4, TRPM2, TRPM4, TRPM6–7, TRPP1–2, and Piezo1–2 in ONH astrocytes (Table 1 and Table 2). Of these, the direct mechanosensitivity of TRPC1 is questioned [80,81], and it does not seem to form functional homomeric channels, though it can interact with other TRPs to form Ca^{2+}-permeable channels [93-96]. Interestingly, a transcript of TRPV4 was detected in ONH astrocytes, which is reported as the calcium entry channel expressed in retinal ganglion cells and activated by hypotonic stimulation [39]. Ryskamp et al. showed that TRPV4 immunoreactivity is not detected in ONH astrocytes, but only one TRPV4 antibody was used in the study [39]. Therefore, it would be valuable to reexamine the expression of TRPV4 protein in ONH astrocytes using other TRPV4 antibodies if possible although many commercial antibodies against mammalian TRP channels show poor quality [32]. Somewhat surprisingly, we were unable to detect transcripts for TRPV1 either in cDNA from whole optic nerve heads or in dissociated single astrocytes, though the retina and the brain yielded a clear signal for this transcript. TRPV1 has been found in ONH astrocytes by a combination of in situ hybridization and immunohistochemistry [91], whereas in another study, using only immunohistochemistry, researchers concluded that the TRPV1 protein in the optic nerve head was localized to the axons [35]. The TRPM7 protein is expressed in the mouse cone outer segments [32], and the channel has also been implicated in mechanosensation in various cell types and can be directly activated by mechanical stress [97-100]. Most astrocytes acutely isolated from the ONH also express TRPP1 and TRPP2, which are known to play an important role in mechanosensation in kidney epithelial cells [101]. TRPP2 can form a Ca^{2+}-permeable cation channel by itself, and TRPP1, a large integral protein, interacts with TRPP2 as a receptor part of a receptor-ion channel complex. Most importantly, ONH astrocytes express Piezo1 and 2, which have recently been established as essential components of distinct stretch-activated channels in mammals [46]. The expression levels of TRPP channels and Piezo2 in the optic nerve are higher compared to the brain and the CC, suggesting possible higher sensitivity to pressure in the region. In addition, Piezo2 expression increases during the progress of glaucoma in DBA/2J mice whereas a less severe injury such as a mild elevation in IOP within a short duration does not induce Piezo2 upregulation, indicating that the glaucomatous ONH might be more sensitive to IOP elevation.

A transient, moderate increase in the IOP (30 mmHg for 1 h) leads to signs of astrocyte reactivity in the ONH but does not apparently damage the ganglion cells [19]. However, a persistently elevated IOP is well known to lead to ganglion cell degeneration and death. Could astrocytes link elevated IOP to retinal ganglion cell injury? Mechanically-induced increase in intracellular calcium concentrations has been demonstrated for astrocytes [41,102,103]. Whether ONH astrocytes react in this way in vivo remains to be tested. Activated astrocytes may release ATP, which could trigger neuronal death of retinal ganglion cells. Acute elevation in IOP induces an increase in extracellular ATP concentration [104,105], and retinal ganglion cells express P2XRs, members of ionotropic (P2X) ATP-gated receptors, which are associated with neuroinflammation and neuronal death [44,106-109]. A recent study suggested mechanosensitive ATP release through pannexin channels, mainly pannexin 1, in ONH astrocytes [87]. Although pannexins open upon membrane stretch [85,87,110], they may not be directly gated by stretch [111,112] and require the involvement of an upstream directly mechanosensitive channel. Another potential mechanism linking astrocyte activation to ganglion cell pathology involves the endothelin system. Astrocytes in culture react to stretch with increased secretion of endothelin-1 [103]. Given the involvement of the endothelin system in glaucoma [17,113], and the ability of endothelin-1 to induce optic neuropathy [114], stretch-induced endothelin secretion by ONH astrocytes may contribute to ganglion cell pathology. None of these mechanisms, of course, would rule out the direct influence of elevated IOP on retinal ganglion cells, possibly mediated by TRP channels that could occur independently of astrocyte reactivity in the optic nerve.

APPENDIX 1. PRIMERS USED FOR CONVENTIONAL AND SINGLE-CELL RT–PCR.

Conventional PCR primers are indicated by an asterisk (*). Nested PCR with two pairs of primers (outer and inner) was used for single-cell RT–PCR experiments. Information of some primer sequences for TRP channels was obtained from a previous study [50] and PrimerBank [51], and the primers are indicated with a dagger (†) and a double dagger (‡), respectively. PrimerBank IDs are presented with the cited primer pairs. To access the data, click or select the words "Appendix 1."

APPENDIX 2. QUANTITATIVE RT–PCR PRIMERS FOR AMPLIFICATION OF TRP CHANNELS AND REFERENCE GENES.

Information of some primer sequences was obtained from PrimerBank [51] and the primers are indicated by an asterisk (*) with PrimerBank ID. To access the data, click or select the words "Appendix 2."

APPENDIX 3. SETS OF PRIMERS AND PROBES FOR TAQMAN REAL-TIME PCR.

To access the data, click or select the words "Appendix 3."

APPENDIX 4. VALIDATION OF CONVENTIONAL PCR PRIMERS.

Primers for TRP channels that were not detected in the ONH were tested in other positive control tissues. M, DNA length marker (100 bp ladder); DRG, dorsal root ganglia. To access the data, click or select the words "Appendix 4."

ACKNOWLEDGMENTS

This work was supported by NIH grants R01EY019703 and R01EY022092, and the Lefler Foundation. The authors wish to thank Dr. Richard Masland for critically reading the manuscript, and Rong Guo, MS, for advice on statistical tests.

REFERENCES

1. Quigley HA. Glaucoma. Lancet 2011; 377:1367-77. [PMID: 21453963].
2. Quigley HA, Addicks EM. Chronic experimental glaucoma in primates. II. Effect of extended intraocular pressure elevation on optic nerve head and axonal transport. Invest Ophthalmol Vis Sci 1980; 19:137-52. [PMID: 6153173].
3. Quigley HA, Addicks EM, Green WR, Maumenee AE. Optic nerve damage in human glaucoma. II. The site of injury and susceptibility to damage. Arch Ophthalmol 1981; 99:635-49. [PMID: 6164357].
4. Balaratnasingam C, Morgan WH, Bass L, Matich G, Cringle SJ, Yu DY. Axonal transport and cytoskeletal changes in the laminar regions after elevated intraocular pressure. Invest Ophthalmol Vis Sci 2007; 48:3632-44. [PMID: 17652733].
5. May CA, Lutjen-Drecoll E. Morphology of the murine optic nerve. Invest Ophthalmol Vis Sci 2002; 43:2206-12. [PMID: 12091418].
6. Morcos Y, Chan-Ling T. Concentration of astrocytic filaments at the retinal optic nerve junction is coincident with the absence of intra-retinal myelination: comparative and developmental evidence. J Neurocytol 2000; 29:665-78. [PMID: 11353290].
7. Sun D, Lye-Barthel M, Masland RH, Jakobs TC. The morphology and spatial arrangement of astrocytes in the optic nerve head of the mouse. J Comp Neurol 2009; 516:1-19. [PMID: 19562764].
8. Johansson JO. Inhibition of retrograde axoplasmic transport in rat optic nerve by increased IOP in vitro. Invest Ophthalmol Vis Sci 1983; 24:1552-8. [PMID: 6197389].
9. Johansson JO. Inhibition and recovery of retrograde axoplasmic transport in rat optic nerve during and after elevated IOP in vivo. Exp Eye Res 1988; 46:223-7. [PMID: 2450768].
10. Howell GR, Libby RT, Jakobs TC, Smith RS, Phalan FC, Barter JW, Barbay JM, Marchant JK, Mahesh N, Porciatti V, Whitmore AV, Masland RH, John SW. Axons of retinal ganglion cells are insulted in the optic nerve early in DBA/2J glaucoma. J Cell Biol 2007; 179:1523-37. [PMID: 18158332].
11. Sun D, Lye-Barthel M, Masland RH, Jakobs TC. Structural remodeling of fibrous astrocytes after axonal injury. J Neurosci 2010; 30:14008-19. [PMID: 20962222].
12. Hernandez MR. The optic nerve head in glaucoma: role of astrocytes in tissue remodeling. Prog Retin Eye Res 2000; 19:297-321. [PMID: 10749379].
13. Lye-Barthel M, Sun D, Jakobs TC. Morphology of astrocytes in a glaucomatous optic nerve. Invest Ophthalmol Vis Sci 2013; 54:909-17. [PMID: 23322566].
14. Johnson EC, Jia L, Cepurna WO, Doser TA, Morrison JC. Global changes in optic nerve head gene expression after exposure to elevated intraocular pressure in a rat glaucoma model. Invest Ophthalmol Vis Sci 2007; 48:3161-77. [PMID: 17591886].
15. Johnson EC, Doser TA, Cepurna WO, Dyck JA, Jia L, Guo Y, Lambert WS, Morrison JC. Cell proliferation and interleukin-6-type cytokine signaling are implicated by gene expression responses in early optic nerve head injury in rat glaucoma. Invest Ophthalmol Vis Sci 2011; 52:504-18. [PMID: 20847120].
16. Qu J, Jakobs TC. The Time Course of Gene Expression during Reactive Gliosis in the Optic Nerve. PLoS ONE 2013; 8:e67094-[PMID: 23826199].
17. Howell GR, Macalinao DG, Sousa GL, Walden M, Soto I, Kneeland SC, Barbay JM, King BL, Marchant JK, Hibbs M, Stevens B, Barres BA, Clark AF, Libby RT, John SW. Molecular clustering identifies complement and endothelin induction as early events in a mouse model of glaucoma. J Clin Invest 2011; 121:1429-44. [PMID: 21383504].
18. Howell GR, Soto I, Zhu X, Ryan M, Macalinao DG, Sousa GL, Caddle LB, MacNicoll KH, Barbay JM, Porciatti V, Anderson MG, Smith RS, Clark AF, Libby RT, John SW. Radiation treatment inhibits monocyte entry into the optic nerve head and prevents neuronal damage in a mouse model of glaucoma. J Clin Invest 2012; 122:1246-61. [PMID: 22426214].
19. Sun D, Qu J, Jakobs TC. Reversible reactivity by optic nerve astrocytes. Glia 2013; 61:1218-35. [PMID: 23650091].
20. Salvador-Silva M, Ricard CS, Agapova OA, Yang P, Hernandez MR. Expression of small heat shock proteins and intermediate filaments in the human optic nerve head astrocytes exposed to elevated hydrostatic pressure in vitro. J Neurosci Res 2001; 66:59-73. [PMID: 11599002].
21. Malone P, Miao H, Parker A, Juarez S, Hernandez MR. Pressure induces loss of gap junction communication and redistribution of connexin 43 in astrocytes. Glia 2007; 55:1085-98. [PMID: 17551925].
22. Mandal A, Shahidullah M, Delamere NA. Hydrostatic pressure-induced release of stored calcium in cultured rat optic

nerve head astrocytes. Invest Ophthalmol Vis Sci 2010; 51:3129-38. [PMID: 20071675].

23. Mandal A, Shahidullah M, Delamere NA, Teran MA. Elevated hydrostatic pressure activates sodium/hydrogen exchanger-1 in rat optic nerve head astrocytes. Am J Physiol Cell Physiol 2009; 297:C111-20. [PMID: 19419999].

24. Hernandez MR, Pena JD, Selvidge JA, Salvador-Silva M, Yang P. Hydrostatic pressure stimulates synthesis of elastin in cultured optic nerve head astrocytes. Glia 2000; 32:122-36. [PMID: 11008212].

25. Yang P, Agapova O, Parker A, Shannon W, Pecen P, Duncan J, Salvador-Silva M, Hernandez MR. DNA microarray analysis of gene expression in human optic nerve head astrocytes in response to hydrostatic pressure. Physiol Genomics 2004; 17:157-69. [PMID: 14747662].

26. Rogers RS, Dharsee M, Ackloo S, Sivak JM, Flanagan JG. Proteomics analyses of human optic nerve head astrocytes following biomechanical strain. Mol Cell Proteomics 2012; 11:M111.012302-[PMID: 22126795].

27. Nilius B, Owsianik G. The transient receptor potential family of ion channels. Genome Biol 2011; 12:218-[PMID: 21401968].

28. Davis MJ, Hill MA. Signaling mechanisms underlying the vascular myogenic response. Physiol Rev 1999; 79:387-423. [PMID: 10221985].

29. Birder LA, Nakamura Y, Kiss S, Nealen ML, Barrick S, Kanai AJ, Wang E, Ruiz G, De Groat WC, Apodaca G, Watkins S, Caterina MJ. Altered urinary bladder function in mice lacking the vanilloid receptor TRPV1. Nat Neurosci 2002; 5:856-60. [PMID: 12161756].

30. Arnadóttir J, Chalfie M. Eukaryotic mechanosensitive channels. Annu Rev Biophys 2010; 39:111-37. [PMID: 20192782].

31. Christensen AP, Corey DP. TRP channels in mechanosensation: direct or indirect activation? Nat Rev Neurosci 2007; 8:510-21. [PMID: 17585304].

32. Gilliam JC, Wensel TG. TRP channel gene expression in the mouse retina. Vision Res 2011; 51:2440-52. [PMID: 22037305].

33. Shen Y, Heimel JA, Kamermans M, Peachey NS, Gregg RG, Nawy S. A transient receptor potential-like channel mediates synaptic transmission in rod bipolar cells. J Neurosci 2009; 29:6088-93. [PMID: 19439586].

34. Morgans CW, Zhang J, Jeffrey BG, Nelson SM, Burke NS, Duvoisin RM, Brown RL. TRPM1 is required for the depolarizing light response in retinal ON-bipolar cells. Proc Natl Acad Sci USA 2009; 106:19174-8. [PMID: 19861548].

35. Leonelli M, Martins DO, Kihara AH, Britto LR. Ontogenetic expression of the vanilloid receptors TRPV1 and TRPV2 in the rat retina. Int J Dev Neurosci 2009; 27:709-18. [PMID: 19619635].

36. Sappington RM, Sidorova T, Long DJ, Calkins DJ. TRPV1: contribution to retinal ganglion cell apoptosis and increased intracellular Ca^{2+} with exposure to hydrostatic pressure. Invest Ophthalmol Vis Sci 2009; 50:717-28. [PMID: 18952924].

37. Ward NJ, Ho KW, Lambert WS, Weitlauf C, Calkins DJ. Absence of transient receptor potential vanilloid-1 accelerates stress-induced axonopathy in the optic projection. J Neurosci 2014; 34:3161-70. [PMID: 24573275].

38. Weitlauf C, Ward NJ, Lambert WS, Sidorova TN, Ho KW, Sappington RM, Calkins DJ. Short-term increases in transient receptor potential vanilloid-1 mediate stress-induced enhancement of neuronal excitation. J Neurosci 2014; 34:15369-81. [PMID: 25392504].

39. Ryskamp DA, Witkovsky P, Barabas P, Huang W, Koehler C, Akimov NP, Lee SH, Chauhan S, Xing W, Renteria RC, Liedtke W, Krizaj D. The polymodal ion channel transient receptor potential vanilloid 4 modulates calcium flux, spiking rate, and apoptosis of mouse retinal ganglion cells. J Neurosci 2011; 31:7089-101. [PMID: 21562271].

40. Sappington RM, Calkins DJ. Contribution of TRPV1 to microglia-derived IL-6 and NFkappaB translocation with elevated hydrostatic pressure. Invest Ophthalmol Vis Sci 2008; 49:3004-17. [PMID: 18362111].

41. Ho KW, Lambert WS, Calkins DJ. Activation of the TRPV1 cation channel contributes to stress-induced astrocyte migration. Glia 2014; 62:1435-51. [PMID: 24838827].

42. Ho KW, Ward NJ, Calkins DJ. TRPV1: a stress response protein in the central nervous system. Am J Neurodegener Dis 2012; 1:1-14. [PMID: 22737633].

43. Ryskamp DA, Redmon S, Jo AO, Krizaj D. TRPV1 and Endocannabinoids: Emerging Molecular Signals that Modulate Mammalian Vision. Cells 2014; 3:914-38. [PMID: 25222270].

44. Križaj D, Ryskamp DA, Tian N, Tezel G, Mitchell CH, Slepak VZ, Shestopalov VI. From mechanosensitivity to inflammatory responses: new players in the pathology of glaucoma. Curr Eye Res 2014; 39:105-19. [PMID: 24144321].

45. Verkhratsky A, Reyes RC, Parpura V. TRP Channels Coordinate Ion Signalling in Astroglia. Rev Physiol Biochem Pharmacol 2014; 166:1-22. [PMID: 23784619].

46. Coste B, Mathur J, Schmidt M, Earley TJ, Ranade S, Petrus MJ, Dubin AE, Patapoutian A. Piezo1 and Piezo2 are essential components of distinct mechanically activated cation channels. Science 2010; 330:55-60. [PMID: 20813920].

47. Bron R, Wood RJ, Brock JA, Ivanusic JJ. Piezo2 expression in corneal afferent neurons. J Comp Neurol 2014; 522:2967-79. [PMID: 24549492].

48. Ikeda R, Cha M, Ling J, Jia Z, Coyle D, Gu JG. Merkel cells transduce and encode tactile stimuli to drive Abeta-afferent impulses. Cell 2014; 157:664-75. [PMID: 24746027].

49. Ikeda R, Gu JG. Piezo2 channel conductance and localization domains in Merkel cells of rat whisker hair follicles. Neurosci Lett 2014; 583:210-5. [PMID: 24911969].

50. Woo SH, Ranade S, Weyer AD, Dubin AE, Baba Y, Qiu Z, Petrus M, Miyamoto T, Reddy K, Lumpkin EA, Stucky CL, Patapoutian A. Piezo2 is required for Merkel-cell

mechanotransduction. Nature 2014; 509:622-6. [PMID: 24717433].

51. Maksimovic S, Nakatani M, Baba Y, Nelson AM, Marshall KL, Wellnitz SA, Firozi P, Woo SH, Ranade S, Patapoutian A, Lumpkin EA. Epidermal Merkel cells are mechanosensory cells that tune mammalian touch receptors. Nature 2014; 509:617-21. [PMID: 24717432].

52. Nakatani M, Maksimovic S, Baba Y, Lumpkin EA. Mechanotransduction in epidermal Merkel cells. Pflugers Arch 2015; 467:101-8. [PMID: 25053537].

53. Faucherre A, Nargeot J, Mangoni ME, Jopling C. piezo2b regulates vertebrate light touch response. J Neurosci 2013; 33:17089-94. [PMID: 24155313].

54. Coste B, Xiao B, Santos JS, Syeda R, Grandl J, Spencer KS, Kim SE, Schmidt M, Mathur J, Dubin AE, Montal M, Patapoutian A. Piezo proteins are pore-forming subunits of mechanically activated channels. Nature 2012; 483:176-81. [PMID: 22343900].

55. Volkers L, Mechioukhi Y, Coste B. Piezo channels: from structure to function. Pflugers Arch 2015; 467:95-9. [PMID: 25037583].

56. Peyronnet R, Martins JR, Duprat F, Demolombe S, Arhatte M, Jodar M, Tauc M, Duranton C, Paulais M, Teulon J, Honore E, Patel A. Piezo1-dependent stretch-activated channels are inhibited by Polycystin-2 in renal tubular epithelial cells. EMBO Rep 2013; 14:1143-8. [PMID: 24157948].

57. Poole K, Herget R, Lapatsina L, Ngo HD, Lewin GR. Tuning Piezo ion channels to detect molecular-scale movements relevant for fine touch. Nat Commun 2014; 5:3520-[PMID: 24662763].

58. McHugh BJ, Buttery R, Lad Y, Banks S, Haslett C, Sethi T. Integrin activation by Fam38A uses a novel mechanism of R-Ras targeting to the endoplasmic reticulum. J Cell Sci 2010; 123:51-61. [PMID: 20016066].

59. McHugh BJ, Murdoch A, Haslett C, Sethi T. Loss of the integrin-activating transmembrane protein Fam38A (Piezo1) promotes a switch to a reduced integrin-dependent mode of cell migration. PLoS ONE 2012; 7:e40346-[PMID: 22792288].

60. Ranade SS, Qiu Z, Woo SH, Hur SS, Murthy SE, Cahalan SM, Xu J, Mathur J, Bandell M, Coste B, Li YS, Chien S, Patapoutian A. Piezo1, a mechanically activated ion channel, is required for vascular development in mice. Proc Natl Acad Sci USA 2014; 111:10347-52. [PMID: 24958852].

61. Yang XN, Lu YP, Liu JJ, Huang JK, Liu YP, Xiao CX, Jazag A, Ren JL, Guleng B. Piezo1 is as a novel trefoil factor family 1 binding protein that promotes gastric cancer cell mobility in vitro. Dig Dis Sci 2014; 59:1428-35. [PMID: 24798994].

62. Libby RT, Anderson MG, Pang IH, Robinson ZH, Savinova OV, Cosma IM, Snow A, Wilson LA, Smith RS, Clark AF, John SW. Inherited glaucoma in DBA/2J mice: pertinent disease features for studying the neurodegeneration. Vis Neurosci 2005; 22:637-48. [PMID: 16332275].

63. Malin SA, Davis BM, Molliver DC. Production of dissociated sensory neuron cultures and considerations for their use in studying neuronal function and plasticity. Nat Protoc 2007; 2:152-60. [PMID: 17401349].

64. Jakobs TC, Libby RT, Ben Y, John SW, Masland RH. Retinal ganglion cell degeneration is topological but not cell type specific in DBA/2J mice. J Cell Biol 2005; 171:313-25. [PMID: 16247030].

65. Kunert-Keil C, Bisping F, Kruger J, Brinkmeier H. Tissue-specific expression of TRP channel genes in the mouse and its variation in three different mouse strains. BMC Genomics 2006; 7:159-[PMID: 16787531].

66. Spandidos A, Wang X, Wang H, Seed B. PrimerBank: a resource of human and mouse PCR primer pairs for gene expression detection and quantification. Nucleic Acids Res 2010; 38:Database issueD792-9. [PMID: 19906719].

67. Lambertsen KL, Gregersen R, Drojdahl N, Owens T, Finsen B. A specific and sensitive method for visualization of tumor necrosis factor in the murine central nervous system. Brain Res Brain Res Protoc 2001; 7:175-91. [PMID: 11356385].

68. Lambertsen KL, Meldgaard M, Ladeby R, Finsen B. A quantitative study of microglial-macrophage synthesis of tumor necrosis factor during acute and late focal cerebral ischemia in mice. J Cereb Blood Flow Metab 2005; 25:119-35. [PMID: 15678118].

69. Andersen CL, Jensen JL, Orntoft TF. Normalization of real-time quantitative reverse transcription-PCR data: a model-based variance estimation approach to identify genes suited for normalization, applied to bladder and colon cancer data sets. Cancer Res 2004; 64:5245-50. [PMID: 15289330].

70. Pfaffl MW, Tichopad A, Prgomet C, Neuvians TP. Determination of stable housekeeping genes, differentially regulated target genes and sample integrity: BestKeeper–Excel-based tool using pair-wise correlations. Biotechnol Lett 2004; 26:509-15. [PMID: 15127793].

71. Jakobs TC, Ben Y, Masland RH. CD15 immunoreactive amacrine cells in the mouse retina. J Comp Neurol 2003; 465:361-71. [PMID: 12966561].

72. Jakobs TC, Ben Y, Masland RH. Expression of mRNA for glutamate receptor subunits distinguishes the major classes of retinal neurons, but is less specific for individual cell types. Mol Vis 2007; 13:933-48. [PMID: 17653033].

73. Choi HJ, Sun D, Jakobs TC. Isolation of intact astrocytes from the optic nerve head of adult mice. Exp Eye Res 2015; In press[PMID: 26093274].

74. Gees M, Colsoul B, Nilius B. The role of transient receptor potential cation channels in Ca^{2+} signaling. Cold Spring Harb Perspect Biol 2010; 2:a003962-[PMID: 20861159].

75. Guo L, Schreiber TH, Weremowicz S, Morton CC, Lee C, Zhou J. Identification and characterization of a novel polycystin family member, polycystin-L2, in mouse and human: sequence, expression, alternative splicing, and chromosomal localization. Genomics 2000; 64:241-51. [PMID: 10756092].

76. Nomura H, Turco AE, Pei Y, Kalaydjieva L, Schiavello T, Weremowicz S, Ji W, Morton CC, Meisler M, Reeders ST, Zhou J. Identification of PKDL, a novel polycystic kidney disease 2-like gene whose murine homologue is deleted in mice with kidney and retinal defects. J Biol Chem 1998; 273:25967-73. [PMID: 9748274].

77. Takumida M, Anniko M. Expression of transient receptor potential channel mucolipin (TRPML) and polycystine (TRPP) in the mouse inner ear. Acta Otolaryngol 2010; 130:196-203. [PMID: 20095091].

78. Djenoune L, Khabou H, Joubert F, Quan FB, Nunes Figueiredo S, Bodineau L, Del Bene F, Burckle C, Tostivint H, Wyart C. Investigation of spinal cerebrospinal fluid-contacting neurons expressing PKD2L1: evidence for a conserved system from fish to primates. Front Neuroanat 2014; 8:26- [PMID: 24834029].

79. Maroto R, Raso A, Wood TG, Kurosky A, Martinac B, Hamill OP. TRPC1 forms the stretch-activated cation channel in vertebrate cells. Nat Cell Biol 2005; 7:179-85. [PMID: 15665854].

80. Dietrich A, Kalwa H, Storch U, Mederos y Schnitzler M, Salanova B, Pinkenburg O, Dubrovska G, Essin K, Gollasch M, Birnbaumer L, Gudermann T. Pressure-induced and store-operated cation influx in vascular smooth muscle cells is independent of TRPC1. Pflugers Arch 2007; 455:465-77. [PMID: 17647013].

81. Gottlieb P, Folgering J, Maroto R, Raso A, Wood TG, Kurosky A, Bowman C, Bichet D, Patel A, Sachs F, Martinac B, Hamill OP, Honore E. Revisiting TRPC1 and TRPC6 mechanosensitivity. Pflugers Arch 2008; 455:1097-103. [PMID: 17957383].

82. Rogers R, Dharsee M, Ackloo S, Flanagan JG. Proteomics analyses of activated human optic nerve head lamina cribrosa cells following biomechanical strain. Invest Ophthalmol Vis Sci 2012; 53:3806-16. [PMID: 22589438].

83. Kalapesi FB, Tan JC, Coroneo MT. Stretch-activated channels: a mini-review. Are stretch-activated channels an ocular barometer? Clin Experiment Ophthalmol 2005; 33:210-7. [PMID: 15807835].

84. Dvoriantchikova G, Ivanov D, Panchin Y, Shestopalov VI. Expression of pannexin family of proteins in the retina. FEBS Lett 2006; 580:2178-82. [PMID: 16616526].

85. Xia J, Lim JC, Lu W, Beckel JM, Macarak EJ, Laties AM, Mitchell CH. Neurons respond directly to mechanical deformation with pannexin-mediated ATP release and autostimulation of P2X7 receptors. J Physiol 2012; 590:2285-304. [PMID: 22411013].

86. Kaja S, Mafe OA, Parikh RA, Kandula P, Reddy CA, Gregg EV, Xin H, Mitchell P, Grillo MA, Koulen P. Distribution and function of polycystin-2 in mouse retinal ganglion cells. Neuroscience 2012; 202:99-107. [PMID: 22155264].

87. Beckel JM, Argall AJ, Lim JC, Xia J, Lu W, Coffey EE, Macarak EJ, Shahidullah M, Delamere NA, Zode GS, Sheffield VC, Shestopalov VI, Laties AM, Mitchell CH. Mechanosensitive release of adenosine 5′-triphosphate through pannexin channels and mechanosensitive upregulation of pannexin channels in optic nerve head astrocytes: A mechanism for purinergic involvement in chronic strain. Glia 2014; 62:1486-501. [PMID: 24839011].

88. Leonelli M, Martins DO, Britto LR. Retinal cell death induced by TRPV1 activation involves NMDA signaling and upregulation of nitric oxide synthases. Cell Mol Neurobiol 2013; 33:379-92. [PMID: 23324998].

89. Zimov S, Yazulla S. Localization of vanilloid receptor 1 (TRPV1/VR1)-like immunoreactivity in goldfish and zebrafish retinas: restriction to photoreceptor synaptic ribbons. J Neurocytol 2004; 33:441-52. [PMID: 15520529].

90. Zimov S, Yazulla S. Vanilloid receptor 1 (TRPV1/VR1) co-localizes with fatty acid amide hydrolase (FAAH) in retinal amacrine cells. Vis Neurosci 2007; 24:581-91. [PMID: 17686199].

91. Ho KW, Sidorova TN, Lambert WS, Calkins DJ. Age and elevated pressure increase astrocyte expression of TRPV1 in retina and optic nerve of the DBA/2J mouse model of glaucoma. ARVO Annual Meeting. Ft. Lauderdale, FL: ARVO E-Abstract; 2011. p. Program #2446.

92. Ho KW, Calkins DJ. Stress-induced upregulation and translocation of TRPV1 in retinal astrocytes. ARVO Annual Meeting. Ft. Lauderdale, FL: ARVO E-Abstracts; 2012. p. Program #6611.

93. Storch U, Forst AL, Philipp M, Gudermann T, Mederos y Schnitzler M. Transient receptor potential channel 1 (TRPC1) reduces calcium permeability in heteromeric channel complexes. J Biol Chem 2012; 287:3530-40. [PMID: 22157757].

94. Ma X, Cheng KT, Wong CO, O'Neil RG, Birnbaumer L, Ambudkar IS, Yao X. Heteromeric TRPV4–C1 channels contribute to store-operated Ca(2+) entry in vascular endothelial cells. Cell Calcium 2011; 50:502-9. [PMID: 21930300].

95. Bai CX, Giamarchi A, Rodat-Despoix L, Padilla F, Downs T, Tsiokas L, Delmas P. Formation of a new receptor-operated channel by heteromeric assembly of TRPP2 and TRPC1 subunits. EMBO Rep 2008; 9:472-9. [PMID: 18323855].

96. Kobori T, Smith GD, Sandford R, Edwardson JM. The transient receptor potential channels TRPP2 and TRPC1 form a heterotetramer with a 2:2 stoichiometry and an alternating subunit arrangement. J Biol Chem 2009; 284:35507-13. [PMID: 19850920].

97. Oancea E, Wolfe JT, Clapham DE. Functional TRPM7 channels accumulate at the plasma membrane in response to fluid flow. Circ Res 2006; 98:245-53. [PMID: 16357306].

98. Numata T, Shimizu T, Okada Y. Direct mechano-stress sensitivity of TRPM7 channel. Cell Physiol Biochem 2007; 19:1-8. [PMID: 17310095].

99. Numata T, Shimizu T, Okada Y. TRPM7 is a stretch- and swelling-activated cation channel involved in volume regulation in human epithelial cells. Am J Physiol Cell Physiol 2007; 292:C460-7. [PMID: 16943238].

100. Roy B, Das T, Mishra D, Maiti TK, Chakraborty S. Oscillatory shear stress induced calcium flickers in osteoblast cells. Integr Biol (Camb) 2014; 6:289-99. [PMID: 24445362].

101. Köttgen M. TRPP2 and autosomal dominant polycystic kidney disease. Biochim Biophys Acta 2007; 1772:836-50. [PMID: 17292589].

102. Niggel J, Sigurdson W, Sachs F. Mechanically induced calcium movements in astrocytes, bovine aortic endothelial cells and C6 glioma cells. J Membr Biol 2000; 174:121-34. [PMID: 10742456].

103. Ostrow LW, Suchyna TM, Sachs F. Stretch induced endothelin-1 secretion by adult rat astrocytes involves calcium influx via stretch-activated ion channels (SACs). Biochem Biophys Res Commun 2011; 410:81-6. [PMID: 21640709].

104. Resta V, Novelli E, Vozzi G, Scarpa C, Caleo M, Ahluwalia A, Solini A, Santini E, Parisi V, Di Virgilio F, Galli-Resta L. Acute retinal ganglion cell injury caused by intraocular pressure spikes is mediated by endogenous extracellular ATP. Eur J Neurosci 2007; 25:2741-54. [PMID: 17459106].

105. Reigada D, Lu W, Zhang M, Mitchell CH. Elevated pressure triggers a physiological release of ATP from the retina: Possible role for pannexin hemichannels. Neuroscience 2008; 157:396-404. [PMID: 18822352].

106. Wheeler-Schilling TH, Marquordt K, Kohler K, Guenther E, Jabs R. Identification of purinergic receptors in retinal ganglion cells. Brain Res Mol Brain Res 2001; 92:177-80. [PMID: 11483255].

107. Zhang X, Zhang M, Laties AM, Mitchell CH. Stimulation of P2X7 receptors elevates Ca^{2+} and kills retinal ganglion cells. Invest Ophthalmol Vis Sci 2005; 46:2183-91. [PMID: 15914640].

108. Hu H, Lu W, Zhang M, Zhang X, Argall AJ, Patel S, Lee GE, Kim YC, Jacobson KA, Laties AM, Mitchell CH. Stimulation of the P2X7 receptor kills rat retinal ganglion cells in vivo. Exp Eye Res 2010; 91:425-32. [PMID: 20599962].

109. Volonté C, Apolloni S, Skaper SD, Burnstock G. P2X7 receptors: channels, pores and more. CNS Neurol Disord Drug Targets 2012; 11:705-21. [PMID: 22963440].

110. Bao L, Locovei S, Dahl G. Pannexin membrane channels are mechanosensitive conduits for ATP. FEBS Lett 2004; 572:65-8. [PMID: 15304325].

111. Reyes JP, Hernandez-Carballo CY, Perez-Flores G, Perez-Cornejo P, Arreola J. Lack of coupling between membrane stretching and pannexin-1 hemichannels. Biochem Biophys Res Commun 2009; 380:50-3. [PMID: 19150332].

112. Seminario-Vidal L, Kreda S, Jones L, O'Neal W, Trejo J, Boucher RC, Lazarowski ER. Thrombin promotes release of ATP from lung epithelial cells through coordinated activation of rho- and Ca^{2+}-dependent signaling pathways. J Biol Chem 2009; 284:20638-48. [PMID: 19439413].

113. Chauhan BC. Endothelin and its potential role in glaucoma. Can J Ophthalmol 2008; 43:356-60. [PMID: 18493277].

114. Chauhan BC, LeVatte TL, Jollimore CA, Yu PK, Reitsamer HA, Kelly ME, Yu DY, Tremblay F, Archibald ML. Model of endothelin-1-induced chronic optic neuropathy in rat. Invest Ophthalmol Vis Sci 2004; 45:144-52. [PMID: 14691166].

Articles are provided courtesy of Emory University and the Zhongshan Ophthalmic Center, Sun Yat-sen University, P.R. China. The print version of this article was created on 14 July 2015. This reflects all typographical corrections and errata to the article through that date. Details of any changes may be found in the online version of the article.